Meniscus Lithography: Evaporation-Induced Self-Organization of Pillar Arrays into Moiré Patterns

Sung H. Kang, Ning Wu,* Alison Grinthal, and Joanna Aizenberg†

School of Engineering and Applied Sciences and Kavli Institute for Bionano Science and Technology, Harvard University, Cambridge, Massachusetts 02138, USA

(Received 14 July 2011; published 20 October 2011)

We demonstrate a self-organizing system that generates patterns by dynamic feedback: two periodic surfaces collectively structure an intervening liquid sandwiched between them, which then reconfigures the original surface features into moiré patterns as it evaporates. Like the conventional moiré phenomenon, the patterns are deterministic and tunable by mismatch angle, yet additional behaviors—chirality from achiral starting motifs and preservation of the patterns after the surfaces are separated—emerge uniquely from the feedback process. Patterning menisci based on this principle provides a simple, scalable approach for making a series of complex, long-range-ordered structures.

DOI: 10.1103/PhysRevLett.107.177802 PACS numbers: 68.47.Pe, 47.61.−k, 81.16.Dn, 81.16.Rf

Pattern formation has been intensely studied across a wide range of length scales both for the insight it provides into the principles of self-organization and for its potential applications in areas such as data storage [1], sensing [2], and wetting [3]. Evaporation-induced patterning has received particular attention [4–6] as a bottom-up, low-energy approach to creating patterns across multiple length scales, as well as for the extremely rich spread of fundamental questions it opens. For example, the ''coffee ring'' effect [7] has been shown to generate a variety of ringed and banded colloidal deposits via evaporation-induced fluid flows that carry particles to the periphery of a droplet. Beyond simple rings and bands, this strategy has been used to produce complex patterned films by placing a shadow mask over the droplet to create regions of free and hindered evaporation [8] or by confining the meniscus to control the ''stick and slip'' motion of capillary flow [9]. In addition to flow-based mechanisms, the capillary forces generated by the menisci between individual particles have attracted interest for their ability to assemble nanopillars [10–13] and other building blocks [14,15] into intricately patterned structures. Although, in each case, the process is inherently mutual—the solid pins the liquid as the liquid moves the solid—the behavior and potential manipulation of the system have rarely been analyzed from this perspective.

While capillary forces can induce local interaction and assembly of individual particles into patterned clusters, in practice, the uniformity of this process over a large area can be difficult to control, and macroscopically ordered, periodic structures assembled by the capillary forces have not been reported. This issue is clearly observed for an array of surface-anchored pillars assembling in an evaporating liquid. As the liquid evaporates, menisci form between the tips of neighboring pillars and generate capillary forces that drive bending and assembly. If the array has uniform spacing, the forces on a given pillar will theoretically be the same in all directions, but in reality, random imperfections and/or instabilities will break the symmetry and cause the pillar to bend in one direction or another [10] [Fig. 1(a)]. This process produces self-assembled bundles whose average size and shape are controlled by the geometric, elastic, and adhesive properties of the pillars, but even a highly periodic array [Fig. 1(b)] produces no long-range order in the symmetry and placement of these bundles, only clusters distributed randomly on the surface [Fig. 1(c)]. To program large-scale order, there have been many efforts to manipulate the geometries (shape, pitch, etc.) [12,13,15] and surface properties of the building blocks [13,16], such that their chemical or structural anisotropy would bias the entire system to assemble into a desired pattern. These approaches, however, have the disadvantage of requiring the building blocks to be specifically designed for each new pattern. An alternative approach would be to place a patterned mask above the array of assembling pillars. As has been shown for colloidal film patterning [8], the mask would impose long-range order on the array by creating regions with varying rates of evaporation. While this method would allow various patterns to be formed from the same pillar array, each pattern would still require a specially designed mask.

Here, we explore a conceptually different approach to masked evaporation that allows a variety of complex patterns to be generated from the same pair of substrate and mask. Instead of using the mask to create a patterned ''shadow'' over the array, we place the mask directly on top of the array such that its raised features come face-to-face with the pillars. As a result, when a liquid is placed in the middle, menisci form between the pillar tips and the mask features. The mask and substrate therefore collectively structure the evaporating liquid at the interface and pattern the menisci that drive bending. To illustrate how this approach leads to long-range order, we analyze the

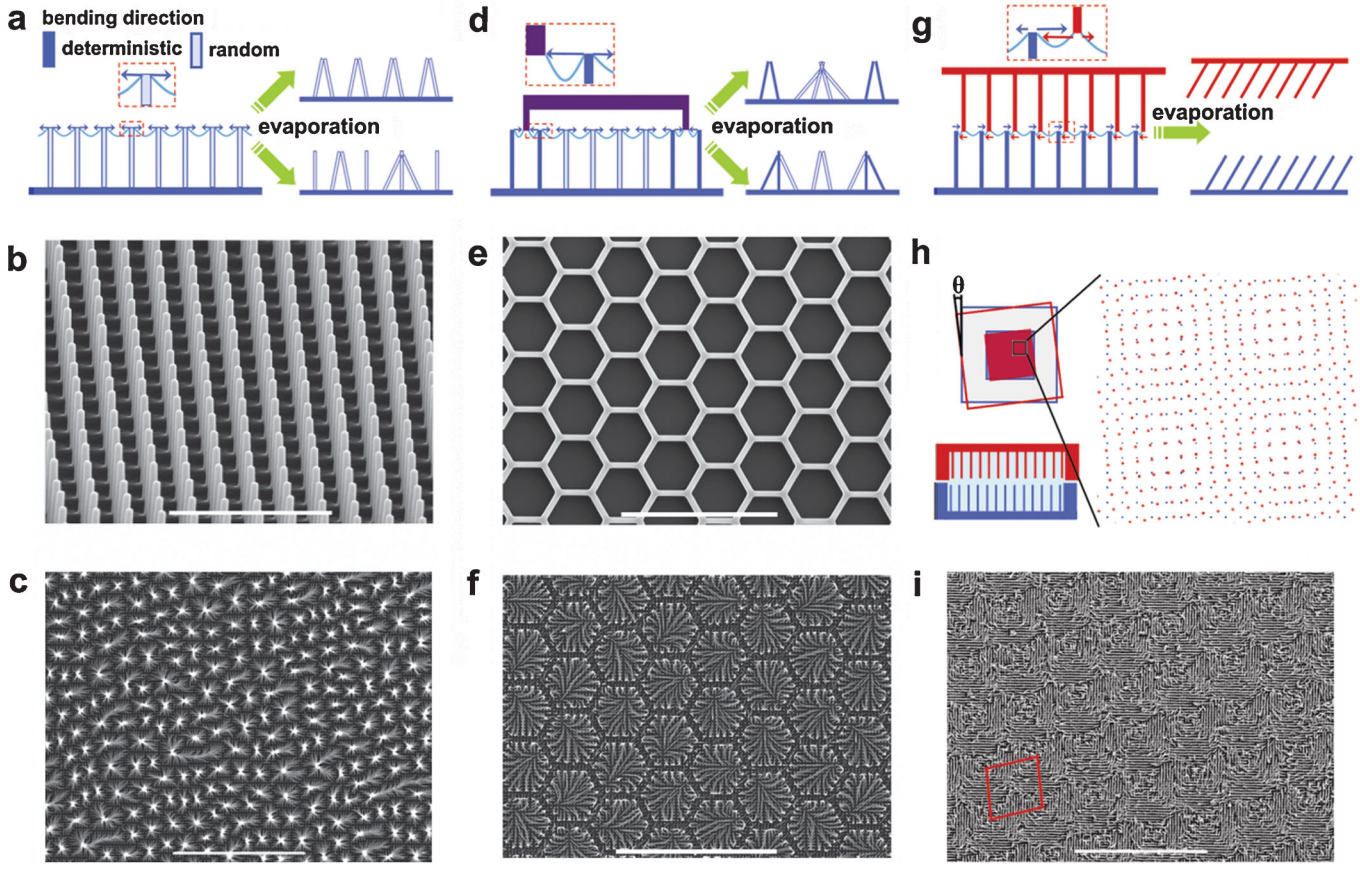

FIG. 1 (color). Pattern formation in pillar arrays upon liquid evaporation. (a)–(c) Maskless process: (a) Schematics of the pillar arrays (side view) before (left) and after (right) evaporative assembly. Dark-colored pillars have deterministic bending directions, while light-colored pillars have random bending directions. Curved blue lines indicate menisci formed between pillars. Arrows indicate the direction of the capillary forces, with relative force magnitudes indicated by length. Note that the final assemblies shown represent only a sampling of the possible patterns that can form, since all the bending directions are random. (b) SEM image of the periodic nanopillar array used in all the experiments. (c) SEM image of the assembled pillar array following evaporation in the absence of a mask. Note the absence of any long-range order. All assembly experiments were performed as described in Ref. [13]. (d)–(f) Evaporation under a superimposed mask with feature spacing larger than that of the array: (d) Schematic of the pattern formation (see text for details); the wetting liquid fills the space between the array and the mask. (e) SEM image of an exemplary honeycomb mask. (f) SEM image of pillars shown in (b) assembled under a honeycomb mask. Note the long-range symmetry determined by the mask, with random patterns within each assembled cell. (g)–(i) Masked evaporation and pattern formation in the sandwich system composed of two identical arrays of pillars: (g) Schematic of the process depicting fully deterministic bending directions in such a system (see text for details). (h) (Left) Schematic of two superimposed pillar arrays (top and side views) corresponding to the case shown in (g). θ is the mismatch angle between the top and bottom lattice axes. (Right) Schematic of the individual pillar positions (top view). Red and blue dots correspond to pillars from top and bottom samples, respectively. Note the appearance of the moiré pattern. (i) SEM image showing the pattern generated from the two identical superimposed arrays after evaporation and remaining as a permanent imprint of the moiré interference on the substrates after separation. The red outline shows a unit cell of the generated pattern. The scale bar is 10 μm for (b) and 100 μm for (c), (e), (f), and (i).

capillary-induced movement of pillars under the patterned mask. When the mask periodicity is larger than that of the underlying array, the pillars closest to the raised features will deterministically bend toward the mask feature defining the overall symmetry of the imprint pattern, but pillars located under the large recessed regions of the mask will still bend randomly [Fig. 1(d)]. The assembly pattern will show long-range order that corresponds to the symmetry of the mask, with random variations within each assembled cell, as demonstrated in Figs. 1(e) and 1(f). As the mask periodicity approaches that of the array, more of the pillars will be adjacent to mask features and will bend in deterministic directions, and fewer pillars will bend randomly. Of particular interest is the situation in which the mask periodicity is the same as that of the array [Fig. 1(g)]. In this case, every pillar will form a meniscus with an adjacent mask feature. Because of the small separation between mask and substrate, each pillar will now be closer to a mask feature than to its neighboring pillars [Fig. 1(g)]. Since the capillary force is inversely proportional to the

spacing [17], the menisci formed between the pillars and mask features will determine the direction of each pillar's movement. All pillars will therefore bend deterministically, making it possible to create a completely controlled collapse pattern. In fact, the mask need not even be different from the substrate—a second copy of the same pillar array can serve as a "mask" with perfect one-to-one feature pairing.

Moreover, this system has all the characteristics of one that gives rise to the moiré effect, whereby two superimposed motifs create unique interference patterns depending on how they are mismatched or placed relative to each other [Fig. 1(h)]. The phenomenon is most commonly observed optically due to the modified behavior of light within the space defined by the new collective pattern. In such cases, there is no feedback: the original motifs are not influenced by the patterned behavior of light, and the moiré pattern disappears when the original motifs are separated. However, for arrays of pillars with a layer of liquid between them, the liquid will not only be patterned through meniscus pinning but will impose force back on both arrays as it evaporates. The mechanical force will therefore translate the collective pattern from the liquid back to the two solid surfaces, and, if the stiffness of the pillars is below the critical value (see Supplemental Material for force estimation [18]), pillars on both the top and bottom surfaces will undergo directional bending and collapse. As a result, identical patterns can be preserved on both the top and bottom samples after separation. Since moiré patterns are highly and predictably sensitive to the rotational angle between the superimposed motifs [19], this would imply that, for our system as well, a wide assortment of patterns can be generated from the same starting components.

To test the potential of moiré interference as a way to generate long-range order and tunable patterns, we used two identical arrays of regularly spaced surface-anchored polymeric nanopillars placed face-to-face with a droplet of ethanol sandwiched between them [Fig. 1(h)]. The arrays consisted of pillars with a radius of 125 nm, a height of 8 μm, and a pitch of 2 μm and were made of epoxy resin (UVO 114 from Epoxy Technology, modulus $\sim$1 GPa) following the procedure described in Ref. [20] (see also Supplemental Material for sample preparation [18]). Upon evaporation, a single control array [Fig. 1(b)] shows no long-range order, preferential bending direction, or periodicity other than the original spacing between the pillars [Fig. 1(c)]. In contrast, the superposition of two such substrates creates a complex, periodic collapse pattern across the scale of the entire sample on both the top and bottom surfaces [Fig. 1(i)].

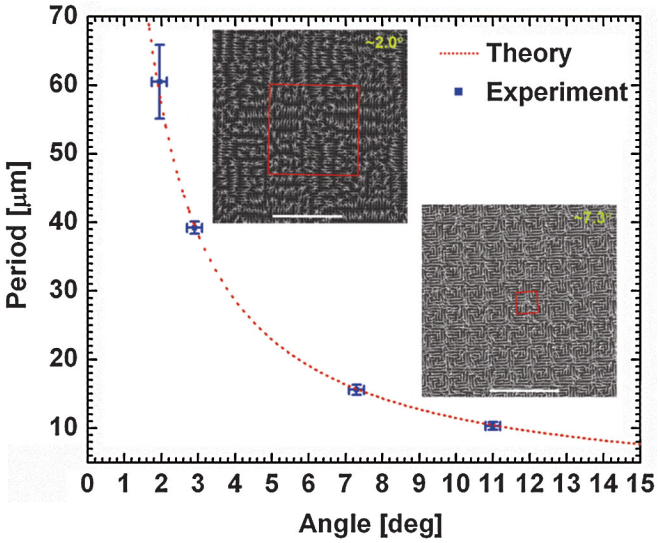

FIG. 2 (color). Plot of the period of the pattern vs the mismatch angle. The dotted line is based on theory (Ref. [21]) and shows good agreement with the experimental results. Error bars indicate standard deviations from at least 5 independent measurements. Representative SEM images of the assembled patterns are shown with their corresponding data points; the number at the upper right indicates the mismatch angle. The red lines indicate unit cells of the generated patterns. The scale bar is 50 μm.

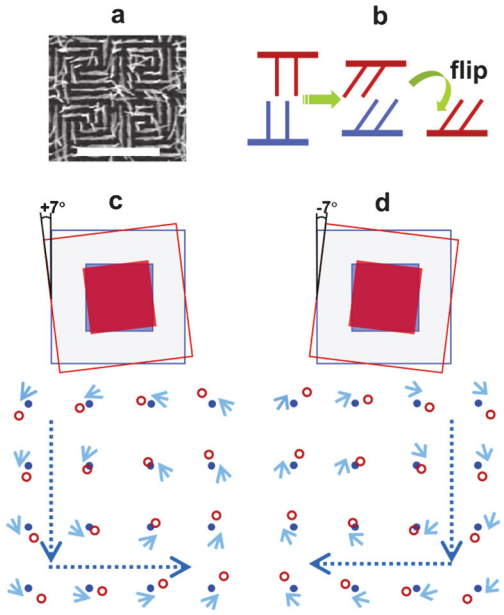

FIG. 3 (color). Appearance of chirality in pillar arrays assembled by meniscus lithography. (a) SEM image showing a spiral collapse pattern. The scale bar is 20 μm. (b) Schematic showing that the patterns formed on the top and bottom arrays have the same chirality. (c),(d) Schematic of the array alignment (top views) and resulting pillar positions depending on the sign of the mismatch angle. A 7° mismatch angle was used as an example. Red hollow circles represent pillars from the top array, while blue solid circles correspond to those from the bottom array. Small arrows indicate the bending directions of the bottom pillars during evaporation, and the large arrows indicate the chirality of the generated patterns.

As for conventional moiré phenomena, the periodicity can be varied by small changes in the rotation angle between the superimposed pillar arrays. We have measured the period of the superlattice obtained with different mismatch angles, as shown in Fig. 2, and the experimental results match well with the theoretical prediction based on optical interference [21]. However, unlike optical moiré patterns, which disappear when the superimposed layers are separated, here the pattern remains preserved in both the top and bottom arrays after they are separated. Although the capillary forces that initially drive pattern formation disappear once the liquid dries, the patterns can be stabilized by plastic deformation of pillars as well as by attractive (e.g., van der Waals) interactions among the deformed pillars or between the pillars and the substrate base.

Meniscus "lithography" by this method also produces patterns with single chirality, which are not observed in either conventional moiré phenomena or traditional evaporation-induced self-assembly. Starting from achiral, cylindrical pillars positioned in a centrosymmetric square array, chirality is introduced as the pillars all tilt either clock- or counterclockwise toward their top neighbors and break the rotational symmetry of the array. This tilting and the resulting collapse occur in a spiral manner [Fig. 3(a)]. The top and bottom samples always have the same chirality as each other and generate two identical collapse patterns, as schematically illustrated in Fig. 3(b). The specific handedness of the chirality can be controlled by the sign of the rotational angle between the two arrays. As shown in the schematic in Figs. 3(c) and 3(d), for opposite rotation directions, the pillars have opposite preferential bending directions prescribed by the overlap of the two arrays, collectively resulting in an opposite handedness. Thus, by simply changing the sign of the rotation angle [Figs. 3(c) and 3(d)], we create patterns with opposite chirality. The handedness remains the same for any angle, as long as the rotation direction does not change.

In order to study the evolution of the pattern formation, we used bright-field microscopy to follow the process of self-assembly in real time as the solvent evaporates between the two superimposed arrays. Figure 4 shows snapshots of the drying process; the bright areas correspond to wet regions, and the dark regions are dry. On a macro-

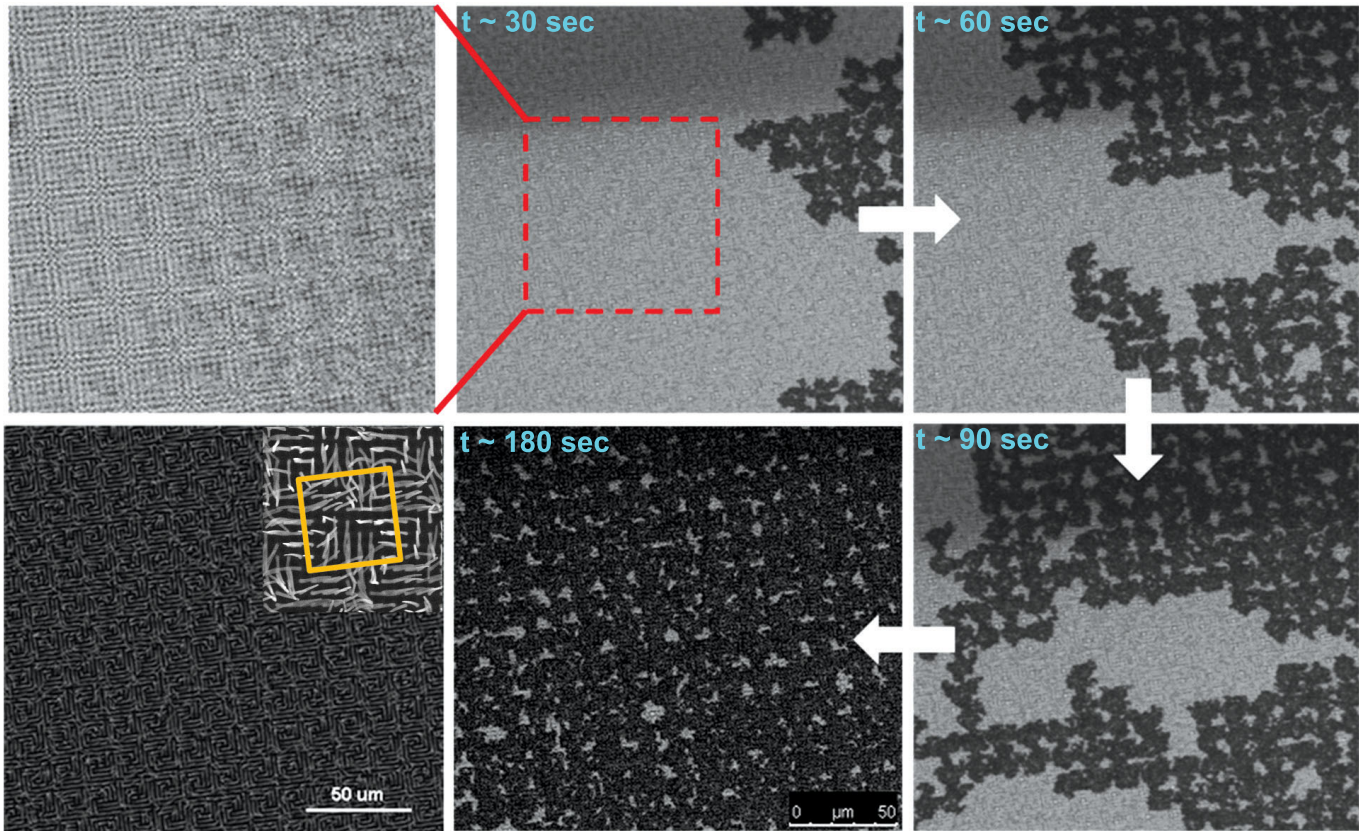

FIG. 4 (color online). Bright-field snapshots of the drying process (first five panels, clockwise from the top left panel) and an SEM image of the resulting pattern (last panel). Dark regions are dry, and light regions are wet. Snapshots were focused at a height approximately corresponding to the pillar tips from the bottom array. The first panel shows the optical micrograph of the moiré interference pattern due to superposition of the top and bottom pillar arrays before drying. The inset in the SEM panel is a zoom-in of the pattern after evaporation, with the square showing a unit cell of the pattern.

scopic scale, as the solvent evaporates, the meniscus recedes from the periphery towards the center of the arrays, with random propagation and generation of pockets of accelerated evaporation due to local imperfections and/or instabilities (Fig. 4). The microscopic movement of the meniscus, however, always follows the superlattice of the moiré pattern imposed by the superposition between the top and bottom pillar arrays. Therefore, a long-range order that corresponds to the moiré superlattice appears as the liquid evaporates, irrespective of the randomness of the evaporation front or the instability distribution. The periodicity of the wet region in the optical image matches with that of the patterns observed in a scanning electron microscope (SEM) image of the corresponding region after drying (Fig. 4).

Our results demonstrate that a liquid sandwiched between two periodic surfaces is reshaped by moiré interference and, in turn, mechanically reconfigures the original surface features to create permanent imprints of the pattern. Patterning takes place via a dynamic feedback mechanism: in our system, the interference pattern arising from the two pillar arrays is read out by an intervening liquid, generating a set of patterned menisci that bend the pillars in predetermined directions upon evaporation. This work not only introduces the rich mathematical theory of moiré phenomena to evaporative and other forms of mechanical force-mediated patterning, but also reveals how a new principle, formation of chiral patterns from achiral starting motifs, can arise in the context of a feedback system. Patterning menisci based on these principles provides a simple, scalable approach, ''meniscus lithography,'' for fabricating a series of complex, long-range-ordered structures from the same starting components. Both periodicity and chirality are easily tuned by small changes in the mismatch angle. While top-down lithography by optical moiré interference has recently been explored [22,23], we show that moiré patterns can evolve spontaneously within a self-assembling system through the direct interplay between solid and liquid components, with no need for specialized optically sensitive materials. Besides two overlapping periodic arrays, this method can also be used to generate controlled assembly patterns from aperiodic structures such as the Glass pattern [24]. Moreover, the idea of meniscus lithography can be extended to various methods of liquid patterning (e.g., using a surface acoustic wave).

This work was supported by the AFOSR under Grant No. FA9550–09-1–0669-DOD35CAP and by the Materials Research Science and Engineering Center under NSF Grant No. DMR-0820484. We acknowledge the use of the facilities at the Harvard Center for Nanoscale Systems supported by NSF Grant No. ECS-0335765. We thank Professor L. Mahadevan and Dr. Philseok Kim for helpful discussions.

*Present address: Department of Chemical and Biological Engineering, Colorado School of Mines, Golden, Colorado 80401, USA.
†Corresponding author.
jaiz@seas.harvard.edu

[1] J. Y. Cheng, C. A. Ross, V. Z. H. Chan, E. L. Thomas, R. G. H. Lammertink, and G. J. Vancso, Adv. Mater. **13**, 1174 (2001).
[2] M. Hu, F. S. Ou, W. Wu, I. Naumov, X. M. Li, A. M. Bratkovsky, R. S. Williams, and Z. Y. Li, J. Am. Chem. Soc. **132**, 12820 (2010).
[3] J. Bico, C. Tordeux, and D. Quere, Europhys. Lett. **55**, 214 (2001).
[4] C. J. Brinker, Y. F. Lu, A. Sellinger, and H. Y. Fan, Adv. Mater. **11**, 579 (1999).
[5] J. X. Huang, F. Kim, A. R. Tao, S. Connor, and P. D. Yang, Nature Mater. **4**, 896 (2005).
[6] N. Chakrapani, B. Q. Wei, A. Carrillo, P. M. Ajayan, and R. S. Kane, Proc. Natl. Acad. Sci. U.S.A. **101**, 4009 (2004).
[7] R. D. Deegan, O. Bakajin, T. F. Dupont, G. Huber, S. R. Nagel, and T. A. Witten, Nature (London) **389**, 827 (1997).
[8] D. J. Harris, H. Hu, J. C. Conrad, and J. A. Lewis, Phys. Rev. Lett. **98**, 148301 (2007).
[9] S. W. Hong, M. Byun, and Z. Q. Lin, Angew. Chem., Int. Ed. Engl. **48**, 512 (2009).
[10] B. Pokroy, S. H. Kang, L. Mahadevan, and J. Aizenberg, Science **323**, 237 (2009).
[11] D. Chandra and S. Yang, Acc. Chem. Res. **43**, 1080 (2010).
[12] H. G. Duan and K. K. Berggren, Nano Lett. **10**, 3710 (2010).
[13] S. H. Kang, B. Pokroy, L. Mahadevan, and J. Aizenberg, ACS Nano **4**, 6323 (2010).
[14] P. A. Kralchevsky and N. D. Denkov, Curr. Opin. Colloid Interface Sci. **6**, 383 (2001).
[15] H. O. Jacobs, A. R. Tao, A. Schwartz, D. H. Gracias, and G. M. Whitesides, Science **296**, 323 (2002).
[16] U. Srinivasan, D. Liepmann, and R. T. Howe, J. Microelectromech. Syst. **10**, 17 (2001).
[17] D. Chandra and S. Yang, Langmuir **25**, 10 430 (2009).
[18] See Supplemental Material at http://link.aps.org/supplemental/10.1103/PhysRevLett.107.177802 for sample preparation, pattern formation and imaging, and force estimation.
[19] I. Amidror, *The Theory of the Moiré Phenomenon, Vol. I: Periodic Layers*, Computational Imaging and Vision Vol. 15 (Kluwer Academic, Dordrecht, 2000).
[20] B. Pokroy, A. K. Epstein, M. C. M. Persson-Gulda, and J. Aizenberg, Adv. Mater. **21**, 463 (2009).
[21] Y. Nishijima and G. Oster, J. Opt. Soc. Am. **54**, 1 (1964).
[22] C. J. Kloxin, T. F. Scott, H. Y. Park, and C. N. Bowman, Adv. Mater. **23**, 1977 (2011).
[23] B. Chen and K. Lu, Langmuir **27**, 4117 (2011).
[24] L. Glass, Nature (London) **223**, 578 (1969).